

SOFT CELLS, KELVIN'S FOAM AND THE MINIMAL SURFACES OF SCHWARZ

G. DOMOKOS, A. GORIELY, Á. G. HORVÁTH AND K. REGŐS

ABSTRACT. Recently, we introduced a new class of shapes, called *soft cells* which fill space as *soft tilings* without gaps and overlaps while minimizing the number of sharp corners. We introduced the *edge bending algorithm* that deforms a polyhedral tiling into a soft tiling. Using this algorithm, we proved that an infinite class of polyhedral tilings can be smoothly deformed into *standard* soft tilings. Here, we demonstrate that certain triply periodic minimal surfaces naturally give rise to non-standard soft tilings. By extending the edge-bending algorithm, we further establish that the soft tilings derived from the Schwarz P and Schwarz D surfaces can be continuously transformed into one another through a one-parameter family of intermediate non-standard soft tilings. Notably, by carrying its combinatorial structure, both resulting tilings belong to the *first order equivalence class* of the (e2) tiling, i.e. the Dirichlet-Voronoi tiling on the body-centered cubic (*bcc*) lattice, highlighting a deep geometric connection underlying these minimal surface configurations. By requiring identical end-tangents for edges in a first order class, we also define *second order equivalence classes* among tilings and prove that there exist exactly two such classes among soft tilings which share the full symmetry group of (e2). We also prove that if we only require tetrahedral symmetry for the cells but also prescribe the presence of at least one planar face, then there exist exactly four second-order classes of soft tilings which are first order equivalents of (e2). Additionally, we construct a one-parameter family of tilings bridging standard and non-standard soft tilings, explicitly including the classic Kelvin's foam structure as an intermediate configuration. This construction highlights that both the soft cells themselves and the geometric methods employed in their generation provide valuable insights into the structural principles underlying natural forms. We also present the soft tiling induced by the gyroid structure.

Key words and phrases. Tessellation, soft cell, Kelvin cell, Dirichlet-Voronoi cell.

CONTENTS

1. Introduction	3
1.1. Motivation and background	3
1.2. Basic notions and the main result	4
2. The EEB algorithm	6
3. The (e2) cell and the proof of Theorem 2	7
3.1. Symmetries and the fundamental domain.	7
3.2. Nodal set and vertex sets	8
3.3. Complete sets of softening equations	8
3.4. Solution of the softening equations	9
3.5. Additional constraints: planar faces	9
3.6. Combining solutions: isolated cells	10
4. Applications	11
4.1. Schwarz minimal surfaces	11
4.2. The Kelvin cell	13
5. Open questions and summary	14
5.1. The gyroid cell	14
5.2. Connecting the Schwarz surfaces	15
5.3. Soft tilings and symmetry groups	17
5.4. Second order families of soft cells	17
5.5. Summary	17
Acknowledgement	18
References	18

1. INTRODUCTION

1.1. Motivation and background. In a recent article [1] we introduced a new class of shapes, called *soft cells* that fill space as *soft tilings* without gaps and overlaps while having no sharp corners at all. Soft tilings, like polyhedral tilings, have a combinatorial structure defined by the adjacency of vertices, edges and faces. However, it is important to note that edges need not be straight and faces need not be planar. We also defined a class of tilings called *polyhedral* that includes, as disjoint subsets, both soft tilings and convex tilings, the latter filling space with convex polyhedra. A key element for the construction of soft tilings is the *edge bending (EB) algorithm* that preserves the combinatorial structure and the location of vertices, maps a subset of convex tilings (to which we refer as *Hamiltonian* tilings) onto a subset of soft tilings, to which we will refer as *standard* soft tilings. Hamiltonian tilings have the property that at every node, the dual of the vertex polyhedron contains a Hamiltonian circuit. Standard soft tilings have the property that at every node, the half-tangents of every incoming edge are collinear.

Although the EB algorithm guarantees the existence of a standard soft tiling M' that is combinatorially equivalent to a given Hamiltonian tiling M , it does not yield a complete set of explicit instructions for the construction of M' . Here we introduce the Extended Edge Bending (EEB) algorithm, which, in principle, is capable of computing, for any given polyhedral tiling M , the entire set $\mathcal{M}(M)$ of soft tilings that share the combinatorial structure and vertex locations of M , while satisfying a prescribed symmetry group and other geometric constraints. Depending on the symmetry group and constraints, the set $\mathcal{M}(M)$ may be finite or infinite and we will compute examples for both cases. The two algorithms are closely related: the EB algorithm guarantees that given a Hamiltonian tiling as input, the EEB algorithm has at least one standard soft tiling as output.

Triply periodic minimal surfaces (TPMS) are embedded minimal surfaces in \mathbb{R}^3 that are invariant under three linearly independent translations, yielding a periodic structure that spans the entire space. The fundamental domains of the translational lattice under which the surface is invariant are unit cells in their own right. Typically, these unit cells are chosen such that the entire surface can be generated by translating the portion within a single cell along three linearly independent lattice vectors. The shape of the unit cell depends on the specific symmetry group of the surface, and the surface within the cell satisfies the minimal surface condition (zero mean curvature) and matches smoothly across opposite faces under the lattice translations. Unit cells are visually not reminiscent of tilings, so, at first sight they are not related to soft cells either. On the other hand, one can construct Voronoi partitions of TPMS [2, 3] which yield soft tilings; we will discuss such constructions related to the Schwarz P and Schwarz D surfaces [4, 2] in Section 4. We will show that the EEB algorithm not only generates the soft tilings associated with these surfaces but it also computes families of soft tilings connecting them. TPMS and their unit cells are critical in crystallographic and materials applications, as they define the repeating geometry and influence mechanical and transport properties when such surfaces are used as microstructure templates for materials [3, 5].

Another interesting natural example is the *Kelvin dry foam*. The corresponding cell, known as the *Kelvin cell*, is a space-filling polyhedral cell proposed by Lord Kelvin in 1887 as a solution to the problem of partitioning space into cells of equal

volume with minimal surface area [6]. It is based on a truncated octahedron—a convex polyhedron with 6 square faces and 8 regular hexagonal faces. In order to satisfy Plateau’s laws for foams, Kelvin’s original construction slightly distorts the regular truncated octahedron into a polyhedric shape with curved faces to reduce the total interfacial area while still filling space without gaps. The Kelvin cell approximates the minimal-area solution for discrete equal-volume polyhedric cells in a foam, whereas TPMS are smooth surfaces with zero mean curvature everywhere.

Here, we will describe and use the EEB algorithm to find non-standard soft tilings which are associated with triply periodic minimal surfaces, including the Schwarz P and Schwarz D surfaces and show that they connect soft tilings with the geometry of optimal dry foams [6].

1.2. Basic notions and the main result. Similarly to the EB algorithm, the output of the EEB algorithm does not fully characterize a soft tiling but only computes both half-tangents for each edge. The remaining features of the shape defined by the curves carrying edges and the surfaces carrying faces can be determined by additional considerations. Motivated by this common feature of the EB and EEB algorithms, below we introduce a classification scheme for polyhedric tilings:

Definition 1. Let M be a polyhedric tiling. Then, the zeroth-order description of M is the combinatorial structure of M . The i -th order description ($i = 1, 2, 3, 4$) of M contains the $(i - 1)$ th order description and the following additional features:

- $i = 1$: the location of nodes,
- $i = 2$: the unit vectors of edge half-tangents,
- $i = 3$: the shape of edges,
- $i = 4$: the shape of faces.

If two tilings M and M' agree up to order k then we say that they are elements of a k -th order equivalence class of tilings. The i -th order description is characterized by the symmetry group Γ_i with fundamental domain f_i and we have $\Gamma_i \leq \Gamma_j$ if $i \geq j$.

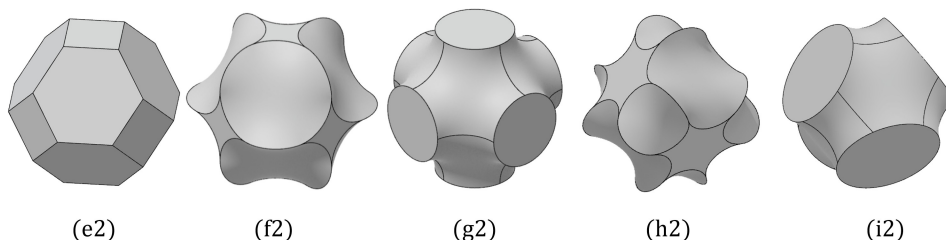


FIGURE 1. The DV-*bcc* cell (called the (e2) cell in [1]) and its four soft versions

Definition 1 naturally leads to a concise and practical new definition of softness:

Definition 2. Let M be a polyhedric tiling with smooth edges and faces. A cell of M is *soft* if each node has at least two half-tangents unit vectors $\mathbf{u}_1, \mathbf{u}_2$ such that $\mathbf{u}_1 \cdot \mathbf{u}_2 = -1$. A tiling is *soft* if each cell in the tiling is soft.

Since softness depends on half-tangents, it is related to the second-order description of the tiling and it is independent of any higher order features. As a consequence, both the EB and the EEB algorithms are of second-order, operating on half-tangents, so they do not determine the shape of cells to higher order. If we want to construct a soft tiling explicitly, we need to specify the shape of its edges and faces, which are respectively included in the third- and fourth-order descriptions. Therefore, to obtain illustrative examples of second-order soft equivalence classes, we will provide the full fourth-order description by imposing that edges are circular arcs with minimal curvature and faces are minimal surfaces.

In this paper we illustrate the EEB algorithm by using the monohedral Dirichlet-Voronoi tiling on the *bcc* lattice as input. In [1] we called this the (e2) tiling and, using the EB algorithm, developed from (e2) the soft, standard (f2) tiling. (Figure 1, first two cells from left). Using the concepts in Definitions 1 and 2 we can now state our two main results for the (e2) tiling:

Theorem 1. *In the first-order equivalence class containing the (e2) tiling there exist exactly two second-order equivalence classes of soft tilings which share the full symmetry group of (e2). Figure 1 shows the soft cells (f2) and (g2) which respectively belong to these two classes.*

Theorem 2. *In the first-order equivalence class containing the (e2) tiling there exist exactly four second-order equivalence classes of soft tilings the cells of which have at least the symmetry group of the regular tetrahedron and have at least one planar face. Figure 1 shows the soft cells (f2), (g2), (h2) and (i2) which respectively belong to these four classes.*

As we can observe, two of these cells are standard ((f2) and (h2)), the other two ((g2) and (i2)) are non-standard. In section 4 we will prove that the second-order equivalence classes containing (g2) and (i2) also contain, respectively, the unit cells of the Schwarz P and Schwarz D surfaces, serving as models of material microstructure, called *mesoatoms* [3, 5].

If we drop the requirement that at least one face should be planar then the EEB algorithm generates a 1-parameter family of soft cells connecting the Schwarz D and Schwarz P unit cells. If we drop the requirement of softness and only require that the quadrangular faces of the (e2) cell remain planar then the EEB algorithm computes a one-parameter family of spacefilling cells that, in addition to the (e2), (f2) and (h2) cells also includes the *Kelvin cell*, serving as the fundamental model of optimal dry foams [6]. This demonstrates that soft cells are significant not only as final geometric forms but also in terms of their underlying geometric genesis which may provide valuable insights into modeling structures in natural phenomena.

We will prove Theorems 1 and 2 in two steps. We first introduce the EEB algorithm in Section 2. Then, in Section 3 we apply the EEB algorithm to the (e2) tiling and compute all solutions under the symmetry and geometric constraints stated in the Theorems. The list of all solutions in Table 2 completes the proofs which is illustrated in Figure 3. After proving Theorems 1 and 2, in Section 4 we will discuss two applications: Schwarz minimal surfaces and the Kelvin foam.

2. THE EEB ALGORITHM

We only describe the EEB algorithm for monohedric, isogonal tilings M where all cells and all nodes are identical, but all steps can be generalized to the case of multiple cells and nodes.

Definition 3. We assume that the polyhedral tiling M is defined to first order, so the symmetry group Γ_1 is known and we also know the symmetry group $\Gamma_2 \leq \Gamma_1$ associated with the second order description. We assume that at each node N cells and K edges meet, so we have K unit vectors as half-tangents, which we call the *nodal set* of M . From the nodal set we can construct N different subsets containing half-tangents, belonging to the N cells. We will refer to these sets of vectors as the N *vertex sets* of M and we denote the size of the vertex sets by v_i , $i = 1, 2, \dots, N$.

Algorithm 1. Using the notions in Definition 3, the steps of the EEB algorithm are the following:

- (1) We identify the fundamental domain f_2 of Γ_2 in the second order description, i.e. we identify a maximal set of unit half tangents \mathbf{u}_i , $i = 1, 2, \dots, f$ which are not related by any transformation of the group Γ_2 .
- (2) Using the set \mathbf{u}_i , $i = 1, 2, \dots, f$ as inputs, we apply symmetry transformations in Γ_2 to construct the nodal set \mathbf{u}_i , $i = 1, 2, \dots, n$, $n \geq f$ of M .
- (3) We pick a pair of half tangents $\mathbf{u}_i, \mathbf{u}_j$ from the nodal set and start writing a list:

$$\mathbf{u}_i \mathbf{u}_j = -1$$

We continue picking pairs and add the corresponding equation to list if the equation does not agree with any previous equation and does not contradict any previous equation. We continue this process until we have at least one equation in every vertex set. At this point, we denote the number of equations by E and we call this system of equations a *complete set of softening equations* of M . The same tiling may have several complete sets of softening equations.

- (4) We let the vectors \mathbf{u}_i , $i = 1, 2, \dots, f$ of the fundamental domain independently run over the boundary of unit sphere. (We may regard the f unit sphere boundaries as a configuration space or *morphospace* [7], containing all possible spacefilling cells of the first order family with given symmetry group.) Since all vectors in the nodal set can be computed via transformation matrices from the fundamental domain, this operation will turn the softening equations into E equations on the sphere in 2 variables and we solve these systems. In fact, the softening equations will be equivalent to eigenvalue problems for the transformation matrices.
- (5) If there are additional, prescribed constraints on the geometry of the cells (e.g. planar faces) then we also solve the corresponding equation systems.
- (6) We combine the solutions guaranteeing soft geometry with those guaranteeing additional constraints.

Remark 1. The existence of a solution of any of these systems is a necessary (but not sufficient) condition for the existence of a soft tiling M' which is equivalent to first order to M , has symmetry group Γ_2 and obeys the prescribed additional geometric constraints. Symmetry is not guaranteed since we may have been able

to compute the nodal set from the fundamental domain by applying only a subset of Γ_2 .

3. THE (e2) CELL AND THE PROOF OF THEOREM 2

In this section we discuss the application of the EEB algorithm to the Dirichlet-Voronoi cell on the *bcc* lattice (the (e2) cell), shown in Figure 2 (see also Figure 1, left image). Our goal is to prove Theorems 1 and 2. We will do the proof in steps numbered as subsections and the numbering of these subsections corresponds *exactly* to the numbering of the steps in Algorithm 1. For steps 1, 2 and 3 the proofs for both Theorems agree. For steps 4, 5 and 6 we will discuss the two proofs separately. The proofs are concluded after Table 2.

Proof. The first-order description of the cell is provided in Table 1, defined as the (e2) cell in [1]. While Figure 2 shows the polyhedral cell defined to fourth order, we only use the first-order information contained in Table 1.

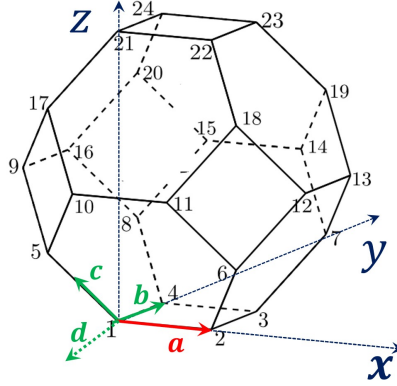


FIGURE 2. The DV-*bcc* cell

3.1. Symmetries and the fundamental domain. The *space group* of the (e2) tiling is $\Gamma_1 = Im\bar{3}m$ (listed as # 229 in [8]), containing the symmetry group of the regular octahedron as a *point group* of order 48. In Theorem 1, for the second order description we require the same symmetry groups. In Theorem 2, for the second order description we require that the soft tiling should have the $\Gamma_2 = Pn\bar{3}m < \Gamma_1$ space group (listed as # 224 in [8]), containing the symmetry group of the regular tetrahedron as a point group of order 24. In both cases (Theorems 1 and 2) the fundamental domain f_2 of the second order description is a single unit vector (i.e. we have $f = 1$) and we pick \mathbf{a} (in the polyhedral tiling $\mathbf{a} = (1, 0, 0)^T$). So we have $\mathbf{u}_1 \equiv \mathbf{a}$.

The nodal set of this tiling consists of 4 vectors (so we have $n = 4$) which we show in Figure 2 at vertex 1, denoted by $\mathbf{a}, \mathbf{b}, \mathbf{c}, \mathbf{d}$, respectively, so we have

Node	x	y	z	Node	x	y	z
1	0	0	0	13	2	1	$2/\sqrt{2}$
2	1	0	0	14	1	2	$2/\sqrt{2}$
3	1	1	0	15	0	2	$2/\sqrt{2}$
4	0	1	0	16	-1	1	$2/\sqrt{2}$
5	-1/2	-1/2	$1/\sqrt{2}$	17	-1/2	-1/2	$3/\sqrt{2}$
6	3/2	-1/2	$1/\sqrt{2}$	18	3/2	-1/2	$3/\sqrt{2}$
7	3/2	3/2	$1/\sqrt{2}$	19	3/2	3/2	$3/\sqrt{2}$
8	-1/2	3/2	$1/\sqrt{2}$	20	-1/2	3/2	$3/\sqrt{2}$
9	-1	0	$2/\sqrt{2}$	21	0	0	$4/\sqrt{2}$
10	0	-1	$2/\sqrt{2}$	22	1	0	$4/\sqrt{2}$
11	1	-1	$2/\sqrt{2}$	23	1	1	$4/\sqrt{2}$
12	2	0	$2/\sqrt{2}$	24	0	1	$4/\sqrt{2}$

TABLE 1. First order description of the (e2) cell

$\mathbf{u}_2 \equiv \mathbf{b}$, $\mathbf{u}_3 \equiv \mathbf{c}$, $\mathbf{u}_4 \equiv \mathbf{d}$. These vectors can be obtained from the vector \mathbf{a} via the following linear transformations:

$$(1) \quad \mathbf{b} = T_b \mathbf{a}, \quad \mathbf{c} = T_c \mathbf{a}, \quad \mathbf{d} = T_{d,i} \mathbf{a}, \quad (i = 1, 2)$$

where

$$(2) \quad T_b = \begin{pmatrix} 0 & 1 & 0 \\ 1 & 0 & 0 \\ 0 & 0 & -1 \end{pmatrix}, \quad T_c = \begin{pmatrix} -\frac{1}{2} & -\frac{1}{2} & \frac{1}{\sqrt{2}} \\ -\frac{1}{2} & -\frac{1}{2} & -\frac{1}{\sqrt{2}} \\ \frac{1}{\sqrt{2}} & -\frac{1}{\sqrt{2}} & 0 \end{pmatrix}$$

$$(3) \quad T_{d,1} = \begin{pmatrix} -\frac{1}{2} & -\frac{1}{2} & +\frac{1}{\sqrt{2}} \\ -\frac{1}{2} & -\frac{1}{2} & -\frac{1}{\sqrt{2}} \\ -\frac{1}{\sqrt{2}} & +\frac{1}{\sqrt{2}} & 0 \end{pmatrix}, \quad T_{d,2} = \begin{pmatrix} -\frac{1}{2} & -\frac{1}{2} & -\frac{1}{\sqrt{2}} \\ -\frac{1}{2} & -\frac{1}{2} & +\frac{1}{\sqrt{2}} \\ -\frac{1}{\sqrt{2}} & +\frac{1}{\sqrt{2}} & 0 \end{pmatrix}.$$

The transformations T_b, T_c apply for both symmetry groups (and thus both Theorems). The transformation producing the vector \mathbf{d} is different in the two cases, $T_{d,1}$ applies for octahedral symmetry, in the proof of Theorem 1 and $T_{d,2}$ applies for tetrahedral symmetry, in the proof of Theorem 2.

3.2. Nodal set and vertex sets. Since we are dealing with a primitive Voronoi tiling, four cells meet at a node so we have $N = 4$. For the same reason, the size of all vertex sets is equal, we have $v_i = 3$, $i = 1, 2, 3, 4$. The vectors $(\mathbf{a}, \mathbf{b}, \mathbf{c})$ compose the vertex set of the cell visible in the figure. There are three other cells meeting at this vertex and their respective vertex sets are $(\mathbf{a}, \mathbf{b}, \mathbf{d})$, $(\mathbf{a}, \mathbf{c}, \mathbf{d})$ and $(\mathbf{b}, \mathbf{c}, \mathbf{d})$.

3.3. Complete sets of softening equations. For this system we can write three different complete sets of softening equations:

$$(4) \quad \mathbf{ab} = -1, \quad \mathbf{cd} = -1$$

$$(5) \quad \mathbf{ac} = -1, \quad \mathbf{bd} = -1$$

$$(6) \quad \mathbf{bc} = -1, \quad \mathbf{ad} = -1.$$

3.4. Solution of the softening equations. Now we make step (4) of the algorithm and let the fundamental domain of the 2nd order description (the unit vector \mathbf{a}) run over the sphere.

3.4.1. Octahedral symmetry: solutions of the equations in the proof of Theorem 1. First we solve system (4). The first equation yields the great circle g_{ab} with unit normal

$$(7) \quad \mathbf{u}_{ab} = \left(\frac{1}{\sqrt{2}}, \frac{1}{\sqrt{2}}, 0 \right)^T,$$

while the second equation has an isolated solution at

$$(8) \quad \mathbf{a}_{cd} = \left(\frac{1}{\sqrt{2}}, -\frac{1}{\sqrt{2}}, 0 \right)^T.$$

Next we solve system (5). The first equation yields the great circle g_{ac} with unit normal

$$(9) \quad \mathbf{u}_{ac} = \left(\frac{1}{2}, -\frac{1}{2}, \frac{1}{\sqrt{2}} \right)^T,$$

while the second equation has an isolated solution at

$$(10) \quad \mathbf{a}_{bd} = \left(\frac{1}{\sqrt{2}}, \frac{1}{\sqrt{2}}, 0 \right)^T.$$

Next we solve system (6). The first equation yields the great circle g_{bc} with unit normal

$$(11) \quad \mathbf{u}_{bc} = \left(-\frac{1}{2}, \frac{1}{2}, \frac{1}{\sqrt{2}} \right)^T,$$

while the second equation has an isolated solution at

$$(12) \quad \mathbf{a}_{ad} = \mathbf{a}_{bd} = \left(\frac{1}{\sqrt{2}}, \frac{1}{\sqrt{2}}, 0 \right)^T.$$

3.4.2. Tetrahedral symmetry: solutions of the equations in the proof of Theorem 2. If we solve the three equation systems (4), (5) and (6) for the unit vector \mathbf{a} , the solutions are great circles which denote respectively by $g_{abcd} \equiv g_{ab}$, $g_{acbd} \equiv g_{ac}$ and $g_{adbcd} \equiv g_{bc}$ the respective unit normals given in (7), (9) and (11). We can observe that g_{acbd} and g_{adbcd} are related by symmetry with respect to the diagonal plane $x = y$, so henceforth we will only compute solutions related to the former.

3.5. Additional constraints: planar faces. In Theorem 1 there are no additional constraints, however, in Theorem 2 we added the constraint that at least one face should remain planar so this subsection is related only to the proof of Theorem 2. For planar face constraints it follows that if a great circle solves the problem then it must lie in the plane of the given face. We solve the corresponding constraint equations to ensure that such a solution actually exists.

The condition that the quadrangular face (1,2,3,4) should remain planar can be written as

$$(13) \quad \mathbf{u}_{quad} \mathbf{a} = 0, \quad \mathbf{u}_{quad} \mathbf{b} = 0,$$

where $\mathbf{u}_{quad} = (0, 0, 1)^T$ is the unit normal of the quadrangular face. The solution of the system (13) is the great circle g_{quad} with unit normal \mathbf{u}_{quad} .

The condition that the hexagonal face (1,2,6,10,11,5) should remain planar can be written as

$$(14) \quad \mathbf{u}_{hex1} \mathbf{a} = 0, \quad \mathbf{u}_{hex1} \mathbf{c} = 0,$$

where $\mathbf{u}_{hex1} = (0, 2/\sqrt{6}, \sqrt{2}/\sqrt{6})^T$ is the unit normals of the hexagonal face. An analogous condition for face (1,4,8,16,9,5) yields $\mathbf{u}_{hex2} = (2/\sqrt{6}, 0, \sqrt{2}/\sqrt{6})^T$. These solutions correspond to the great circles g_{hex1}, g_{hex2} with respective unit normals $\mathbf{u}_{hex1}, \mathbf{u}_{hex2}$.

3.6. Combining solutions: isolated cells. Now we can conclude the proofs of Theorems 1 and 2 and we discuss these separately.

3.6.1. Octahedral symmetry: completing the proof of Theorem 1. As we can observe, all equation systems yield one great circle and one isolated point on that great circle. This would provide three isolated solutions, however, the solutions of the systems (5) and (6) are identical, so we obtain two isolated solutions, given in (8) and (10), corresponding to the soft cells (f2) and (g2), respectively, listed in Table 2. Figure 3 illustrates, among others, these 2 soft cells along with the great circles g_{abcd}, g_{acbd} on the plane (ϕ, θ) of the Euler angles.

3.6.2. Tetrahedral symmetry: completing the proof of Theorem 2. We observe that all equation systems yield a one-parameter family of solutions, each family being equivalent to a great circle on the unit sphere. To obtain *isolated* solutions we regard suitable *pairs* of these great circles. We pick pairs in such a manner that for each pair one great circle should guarantee the softness, the other should guarantee at least one planar face. We also consider that the great circles g_{acbd} and g_{adbc} are related by the $x \leftrightarrow y$ reflection symmetry, so it is sufficient to consider one of them to obtain all solutions which are not related by a symmetry transformation. Using these considerations we obtained the four soft solutions (f2), (g2), (h2) and (i2), listed in Table 2. The polyhedral cell (e2) is listed in the first row of the table, as it can be obtained by combining the solutions for planar hexagonal and planar quadrangular faces. In the table we not only identify the great circles the intersection of which determine the given cell but also give the Cartesian coordinates and the corresponding Euler angles for the unit vector \mathbf{a} . From the latter the entire tiling can be reconstructed to second order by the action of the space group $\Gamma_2 = Pn3m$.

Figure 3 is illustrating both the four soft cells satisfying all constraints, but also the polyhedral cell (e2) and the great circles $g_{abcd}, g_{acbd}, g_{hex1}, g_{hex2}$ and g_{quad} on the plane (ϕ, θ) of the Euler angles.

We note that the listed solutions are only defined to second order, i.e each soft cell that appears as an isolated point on the plane of Euler angles represents an infinite set of soft cells with identical vertex locations and identical half-tangents for the edges. The cells appearing in Figures 1, 3 are particular elements of this infinite sets. We picked these elements by using circular arcs as edges and minimal surfaces as faces.

Name	great circles			a_x	a_y	a_z	ϕ	θ	σ
(e2)	g_{hex}	g_{quad}		1	0	0	$\pi/2$	0	0
(f2)	g_{adb}	g_{quad}	g_{acbd}	$1/\sqrt{2}$	$1/\sqrt{2}$	0	$\pi/2$	$\pi/4$	0.331
(g2)	g_{adb}	g_{quad}		$1/\sqrt{2}$	$-1/\sqrt{2}$	0	$\pi/2$	$-\pi/4$	0.333
(h2)	g_{adb}	g_{hex1}	g_{acbd}	1/2	-1/2	$1/\sqrt{2}$	$\pi/4$	$-\pi/4$	0.464
(i2)	g_{adb}	g_{hex2}		$\sqrt{3}/2$	$\sqrt{3}/6$	$1/\sqrt{6}$	$\cos^{-1}(1/\sqrt{6})$	$\tan^{-1}(1/3)$	0.474

TABLE 2. The polyhedral (e2) cell and all 4 first order equivalent soft cells with at least tetrahedral symmetry and at least one planar face, given with the $[x, y, z]$ coordinates of the unit vector \mathbf{a} (cf. Figure 2) and with Euler angles, where $\theta = 0, \phi = 0$ coincide respectively with the x and z axes of the Cartesian system shown on Figure 2. Last column: softness value $0 \leq \sigma \leq 1$, as defined in [1].

□

4. APPLICATIONS

4.1. Schwarz minimal surfaces. As previously introduced, Triply Periodic Minimal Surfaces (TPMS) are smooth, continuous, minimal surfaces (i.e. with zero mean curvature) characterized by three independent, periodic directions in three-dimensional space. Beyond their unique geometrical role [9], highly relevant as models in material science [3, 5]. While the primary geometric interpretation of a TPMS is that of an *interface*, the same object can also be interpreted as a *tiling*. This interpretation is certainly not new. While many aspects have been described both from the geometrical [2] and physical [3] perspective, we are not aware of a clear definition connecting TPMS to tilings. Hence, so our first goal is to define this connection.

TPMS generate a special binary partition of 3D space: each partition is a *labyrinth* formed by a tubular system with infinitely many branching points [2]. Hence, a given TPMS gives rise to two tubular labyrinths with branching points. Both tubular labyrinths can be collapsed onto a respective *skeletal graph* the nodes of which correspond to branching points (see Figure 4, panels (a1),(b1)), so TPMS are associated to a pair of infinite skeletal graphs. Since TPMS are smooth, so the cross section of the tubes is also a smooth curve. This implies a simple

Observation 1. The Voronoi partition of a labyrinth of a TPMS labyrinth with respect to the nodes of its skeletal graph results in a soft tiling. We will call the cell of this tiling the Voronoi cell associated with the TPMS. If the two labyrinths are identical and the skeletal graph has identical edges and vertices then this tiling is monohedric and the Voronoi cell of the tiling is a monohedric soft cell. Monohedric Voronoi tilings have been used as physical models of materials structure, and they were called *mesoatoms* [3].

The first TPMS was identified by Riemann [10] and independently by Schwarz [4] who also found another example; these two surfaces are dubbed as the Schwarz D (“diamond”) and the Schwarz P (“primitive”) surface, respectively. Panels

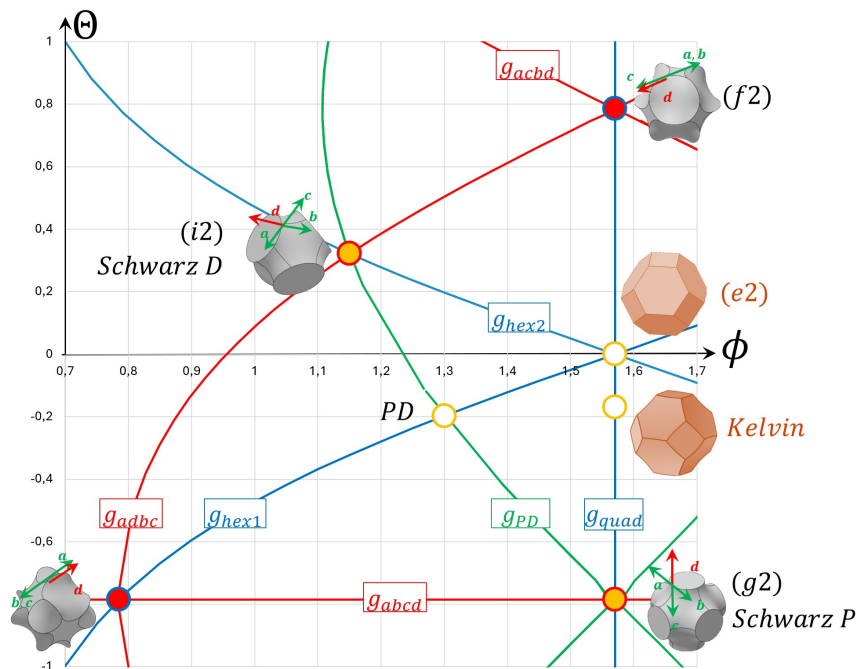


FIGURE 3. All solutions of the softening equations for the polyhedral (e2) cell shown in Figure 2, plotted on the plane (ϕ, θ) of Euler angles ($\theta = 0, \phi = 0$ coinciding respectively with the x and z axes of the Cartesian system shown on Figure 2). Red lines: great circles solving complete sets of softening equations. Blue lines: great circles solving constraint equations which keep faces planar. Green lines: great circles connection non-standard soft cells. Blue dots with red fill: standard soft cells identified by the intersection of two red lines and one blue line. Red dots with yellow fill: non-standard soft cells defined by the intersection of one blue and one red line. Yellow dots with white fill: non-soft cells. For detailed data on cells (e2), (f2), (g2), (h2), (i2) see Table 2. For data on the Kelvin cell and the PD cell see Table 3. For better visibility, nodal set **a, b, c, d** is shown on vertex 21 instead on vertex 1.

(a1) and (b1) of Figure 4 show a Voronoi cell of these surfaces along with a portion of their skeletal graphs. For both the Schwarz P and the Schwarz D surface, the dual labyrinth is identical to the one shown in the figure and the skeletal graphs are isogonal, i.e. their nodes are identical. The degree n of their nodes is characteristic of the symmetry of their Voronoi cells, as it defines the number of neighbor cells in the same labyrinth. In the case of the Schwarz P surface we have a node of degree $n = 6$ with cubic symmetry and in the case of the Schwarz D surface we have $n = 4$ with tetrahedral symmetry. Remarkably, these surfaces are related to the soft tilings we demonstrated in Section 2:

Proposition 1. *The Voronoi cells of the Schwarz P and Schwarz D minimal surfaces are equivalent to second order to the soft cells (g2) and (i2), respectively.*

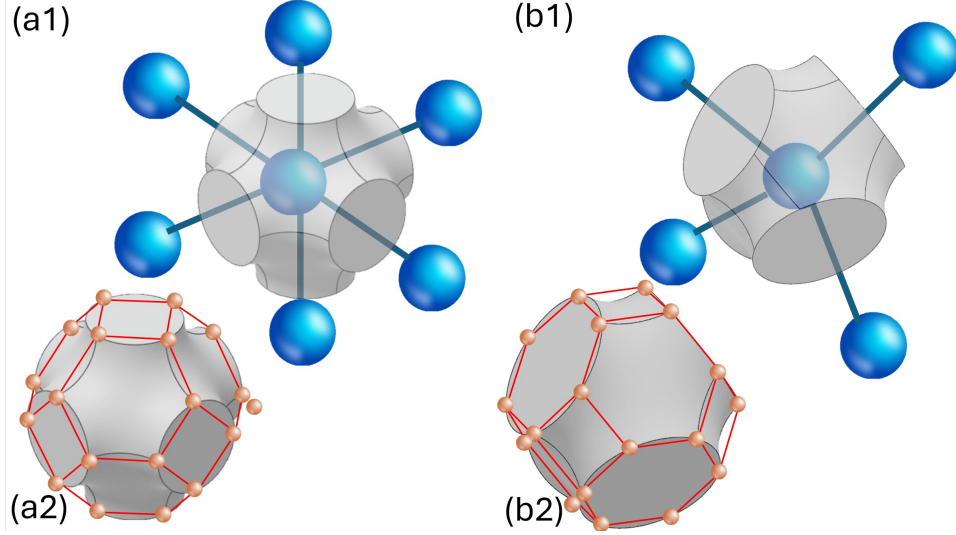


FIGURE 4. Discrete structures on triply periodic minimal surfaces. Upper row, (a1)-(b1): Unit cells and skeletal graphs. Bottom row, (a2)-(b2): Unit cells carrying the vertices of the skew polyhedron $\{6|4, 4\}$. Left column, (a1)-(a2): Schwarz P surface. Right column, (b1)-(b2): Schwarz D surface.

Proof. Here we regard the soft tilings defined by two TPMS: the Schwarz P and Schwarz D surfaces, illustrated in Figure 4. According to Schoen [2], the unit cell of the Schwarz P surface has octahedral symmetry (see also [11]) and the unit cell of the Schwarz D surface has tetrahedral symmetry and both are equivalent to the (e2) tiling to first order: they carry the vertices of the regular map $\{6, 4|4\}$ [12] which is, to third order, composed of the truncated octahedra (see panels (a2) and (b2) of Figure 4). Based on Observation 1 we also know that both Schwarz Voronoi cells have n smooth, planar faces. According to Theorem 2, there are 4 soft tilings which are first order equivalents of the (e2) tiling and also carry planar faces. Two of these tilings has a unit cell where the planar faces are non-smooth: these are the standard soft cells (f2) and (h2). The only remaining two cells are (g2) and (i2) so the two Schwarz cells have to be equivalent to these cells to second order. \square

4.2. The Kelvin cell. A notable, historic example for curved tilings is the geometric model of dry foams where the tiling has to obey Plateau's Laws [13]. While the structure of foams is strongly reminiscent of polyhedral tilings, there is no space-filling polyhedron meeting this requirement. William Thomson (Lord Kelvin), when faced with this dilemma, proposed to *slightly modify* the truncated octahedron by deforming its edges [6]. The result is a monohedric tiling that became known as the *Kelvin Foam* and its cell as the *Kelvin Cell* (see Figure 5). The latter is, to

this date, is believed to have the smallest surface area among solids that tile space [14, 15, 16].

The Kelvin foam is identical to the (e2) tiling (see Figure 2) to first order and it is invariant under the $\Gamma_1 = Im3m$ space group. Similarly to the previously discussed soft cells, the fundamental domain is represented by the vector \mathbf{a} . Below we compute the coordinates of \mathbf{a} , both in the Cartesian (x, y, z) system as well in Euler angles.

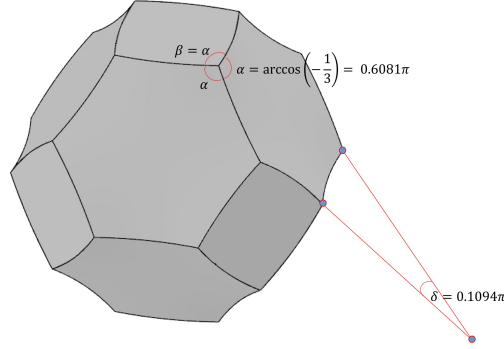


FIGURE 5. The Kelvin Cell

The geometric constraint equations defining the Kelvin cell to second order describe Plateau's law for the edges, prescribing that all edges meet at identical angles, yielding:

$$(15) \quad \mathbf{ab} = \mathbf{ac} = \mathbf{ad} = \mathbf{bc} = \mathbf{bd} = \mathbf{cd}.$$

We find that from the (15) system the equation $\mathbf{ac} = \mathbf{ad}$ yields

$$(16) \quad a_z = 0.$$

Also, from (15) it follows that the 4 vectors point to the vertices of a regular tetrahedron, yielding

$$(17) \quad \mathbf{ab} = \mathbf{ac} = \mathbf{ad} = \mathbf{bc} = \mathbf{bd} = \mathbf{cd} = -1/3.$$

If we pick $\mathbf{ab} = -1/3$ from (17) and we substitute (16) into this equation, we get the solution displayed in Table 3. This also satisfies (13), the Kelvin cell has $Im3m$ space symmetry, the tiling is invariant under the $z \rightarrow -z$ reflection, implying that the quadrangular faces of the cell are planar.

We observe that the g_{quad} great circle contains a one parameter family of space-filling cells which are first order equivalents of the (e2) cell and which connect the latter with the (f2) standard soft cell and the Kelvin cell.

5. OPEN QUESTIONS AND SUMMARY

5.1. The gyroid cell. The Schwarz P and D surfaces are related by the continuous bending transformation described in 1853 by Ossian Bonnet [17]. They are members of a one-parameter family of surfaces, called the Bonnet family, with free parameter α , at the values $\alpha = 0$ (D) and $\alpha = \pi/2$ (P). Beyond the Schwarz P and D

Name	great circles		a_x	a_y	a_z	ϕ	θ
Kelvin	g_{quad}		$\frac{1}{\sqrt{1+(2\sqrt{2}-3)^2}}$	$\frac{2\sqrt{2}-3}{\sqrt{1+(2\sqrt{2}-3)^2}}$	0	$\frac{\pi}{2}$	$\tan^{-1}(2\sqrt{2}-3)$
PD	g_{PD}	g_{hex1}	$\frac{5}{\sqrt{28}}$	$\frac{-1}{\sqrt{28}}$	$\frac{\sqrt{2}}{\sqrt{28}}$	$\cos^{-1}\left(\frac{1}{\sqrt{14}}\right)$	$\tan^{-1}\left(-\frac{1}{5}\right)$

TABLE 3. The Kelvin cell and the PD cell. See Figure 3 for the representation on the plane of the Euler angles.

surfaces there one single member of this family (at $\alpha \approx 0.663225$) which has no self-intersections: this TPMS, discovered by Alan Schoen [2], is called the gyroid.

While the gyroid is included in the same Bonnet family as the Schwarz P and D surfaces, its geometry is radically different. While the gyroid also gives rise to two identical labyrinths (differing only in handedness), however, the nodes of the skeletal graphs are of degree $n = 3$ and in a unit cube there are 8 such nodes (see panel (a) of Figure 6, based on Figure 1e in [18]). According to Schoen [2], the space group of the gyroid surface is the $I4_132$ group (# 214 in the list provided in [8]).

Panel (a) of Figure 6 shows the qualitative picture of one labyrinth of the gyroid. Using Observation 1 one can obtain the soft, monohedric G cell in panel (b). We computed the softness value σ for this cell and found $\sigma = 0.576$ which is the highest value computed so far for any monohedric soft cell. Subsequently, by removing all edges and all faces, we took the first-order approximation of this soft cell and obtained the *non-convex*, spacefilling polyhedron, shown in panel (c). (Recall, that in the case of the Schwarz P and Schwarz D surfaces this operation results in the convex (e2) cell.) In the next step, we used the nodes P_i of the labyrinth to construct the Voronoi tiling of 3D space, resulting in the convex polyhedron shown in panel (d). Although the difference between the polyhedra in panels (c) and (d) is small, it remains clearly noticeable. Importantly, the same procedure of constructing a Voronoi tiling of space with respect to the nodes of the labyrinth, yields, for both Schwarz surfaces, the (e2) cell, which precisely matches the polyhedral approximation of the soft Voronoi cells.

Schoen [2] noticed this peculiar property for the gyroid, he found the convex polyhedron in panel (d), identified it as the L_2V_{17} polyhedron and called the corresponding monohedral tiling a *toy model* of the gyroid. Apparently, Schoen was aware of the difference between the polyhedra in panels (c) and (d) of Figure 6 and he also commented that the gyroid is not associated directly with any convex tiling.

In principle, the EEB algorithm can compute all soft cells that are first-order equivalents of a given polyhedral tiling. However, in the case of the nonconvex polyhedron shown in panel (c), this computation appears to be particularly challenging. Nonetheless, determining whether another soft cell exists that is first-order equivalent to the soft gyroid cell is an intriguing open question, given the significant role the gyroid structure plays in characterizing material microstructures [3].

5.2. Connecting the Schwarz surfaces. As noted earlier, the Schwarz surfaces P and D represent the endpoints of a one-parameter family of minimal surfaces originally described by Bonnet [17]. Such one-parameter families, in which one soft cell continuously transforms into another, are not merely mathematical curiosities;

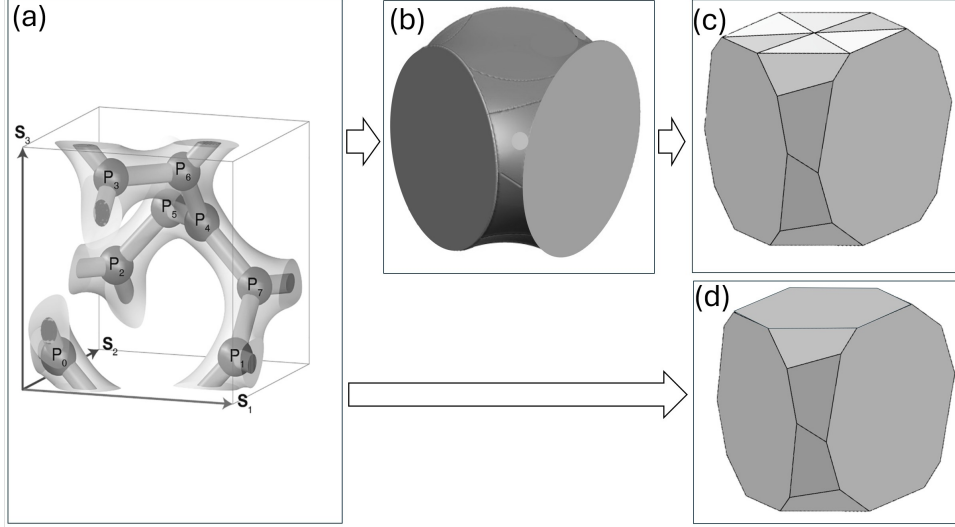


FIGURE 6. The gyroid cell. (a) One labyrinth of the gyroid with $n = 3$ order nodes P_i , $i = 0, 1, 2, 3, 4, 5, 6, 7$ (see [18], Figure 1e). (b) Soft, space-filling G cell, obtained by Voronoi decomposition of the gyroid labyrinth [3]. (c) Non-convex, space-filling mono-hedral cell obtained by first order approximation of the G cell. (d) Convex, space-filling mono-hedral cell L_2V_{17} , obtained by Voronoi decomposition of 3D space using the nodes P_i [2].

indeed, they have also been observed experimentally [19], highlighting their practical relevance in physical systems. The interpretation of both Schwarz surfaces as soft tilings (g2) and (i2) admits additional one-parameter connections between them, which we describe below.

Both (g2) and (i2) are first order equivalents of the (e2) tiling satisfying two additional constraints: both result from the Voronoi decomposition of tubular labyrinths and both are soft tilings. If we relax either the first or the second of the latter two properties then we find one-parameter families of first-order (e2) tilings that connect the Schwarz P to the Schwarz D surface.

First we relax the Voronoi construction: this is equivalent of relaxing the constraint of planar faces. This results in the connection (g2) \rightarrow (h2) \rightarrow (i2), consisting entirely of *soft tilings*. This connection, along the great circles g_{abcd} and g_{adbc} is marked by red lines in Figure 3. Next, we relax the softness condition and keep the constraint of planar faces. This results in the connection (g2) \rightarrow (e2) \rightarrow (i2), consisting entirely of suitably defined *Voronoi tilings*. This connection, along the great circles g_{quad} and g_{hex2} is marked by blue lines in Figure 3. We may also relax *both* conditions. In this case any one-parameter curve on the unit sphere passing through (g2) and (i2) may be chosen. The shortest path is the great circle g_{PD} , marked by green line in Figure 3, connecting the soft cells (g2) and (i2). We

computed the unit normal as

$$(18) \quad \mathbf{u}_{PD} = \left(\frac{1}{\sqrt{12}}, \frac{1}{\sqrt{12}}, -\frac{2}{\sqrt{6}} \right).$$

While this solution appears to provide the most natural link between first-order (e2) tilings, it remains unclear what specific geometric constraint it imposes on the shape of the corresponding cell. If we consider the intersection of the solutions g_{PD} and g_{hex1} , we obtain an isolated solution, which we refer to as the *PD-cell*. The coordinates of this cell are presented in Table 3. Notably, the PD-cell is not soft; the relevant scalar products can be explicitly calculated as $\mathbf{ab} = -3/7$, $\mathbf{ac} = 1/7$, and $\mathbf{bc} = -5/7$.

5.3. Soft tilings and symmetry groups. Observation 1 identified the soft cells generated by Voronoi partitions of TPMS and in Proposition 1 we were able to identify the Voronoi cell of the Schwarz P and Schwarz D surfaces with the soft cells (g2) and (i2), both being first order equivalent to the truncated octahedron (e2) cell. The soft tilings associated with these cells exhibit the full symmetry of their corresponding minimal surfaces, as their vertices align precisely with those of the regular map $\{6, 4|4\}$ described by Coxeter [12]. Furthermore, TPMS accommodate various other regular maps and infinite polyhedra, each defining distinct soft monohedric tilings with reduced symmetry groups. These discrete structures thus enable the generation of soft monohedric tilings characterized by a range of smaller symmetry groups.

We also remark that, according to Theorem 1, the soft tilings (f2) and (g2) inherit the full symmetry group of the (e2) polyhedral tiling, the latter being one of the five Dirichlet–Voronoi cells of point lattices [20, 21]. An examination of the remaining four Dirichlet–Voronoi cells shows that no corresponding soft tiling exists that preserves the full symmetry group of their polyhedral mosaics. An intriguing open question is whether, aside from the (f2) and (g2) tilings, there exist additional soft tilings that fully inherit the symmetry of their respective polyhedral tilings.

5.4. Second order families of soft cells. Although we only used its second order structure, the (e2) cell in Figure 1 is determined to fourth order and the same holds for the Kelvin cell in Figure 5. In contrast, the 4 soft cells (f2), (g2), (h2) and (i2) appearing in Theorem 2 and later in our computations are, strictly speaking, only determined to second order. The images shown in Figures 1, 3 are examples of these second order families where we complemented the second order structure by circular edges and minimal surfaces as faces, to obtain the full geometry of the cells. Indeed, the proof of Proposition 1 relies precisely on the insight that specifying the exact geometric form of the Schwarz P and D cells is unnecessary to identify them as members of the (g2) and (i2) families. Visually, however, the differences between the Schwarz cells and the illustrated examples of the (g2) and (i2) families are minimal. To emphasize that our analysis is limited to second-order considerations and thus does not entirely constrain the cell shapes, we provide two additional examples of cells belonging to the (g2) family in Figure 7.

5.5. Summary. In this paper, we introduced and described the EEB algorithm, which not only computes the shapes of soft cells up to the half-tangents of their edges, but also, in principle, is capable of identifying *all* soft cells sharing the vertices

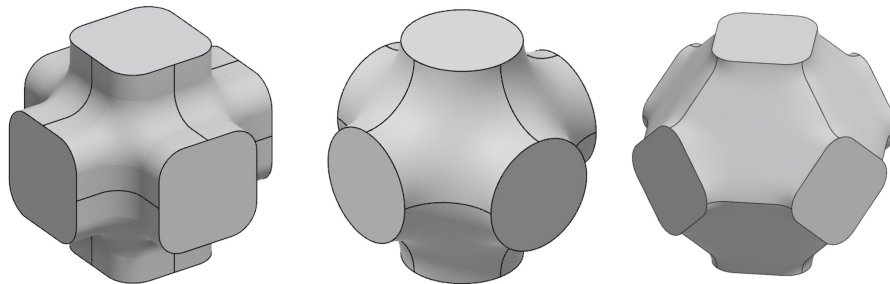


FIGURE 7. Three members of the second order family (g_2) of soft cells, containing also the Schwarz P unit cell

of a given polyhedral tiling. To demonstrate the effectiveness of this algorithm, we applied it to the Dirichlet-Voronoi tiling of the *bcc* lattice. We proved that exactly two types of soft cells exist, determined up to the half-tangents of their edges, which share the vertices and the full symmetry group of the polyhedral tiling. We also proved that exactly four types of soft cells exist, determined up to the half-tangents of their edges, that share the vertices of this monohedral tiling, exhibit at least tetrahedral symmetry, and possess at least one planar face. Furthermore, we established that two of these soft cells correspond precisely to the Voronoi cells associated with the Schwarz P and Schwarz D minimal surfaces, respectively.

The EEB algorithm has successfully identified soft cells that differ fundamentally from the standard examples previously illustrated in [1]. This discovery significantly expands the spectrum of potential applications and invites exciting new explorations into the diversity of soft-cell geometries yet to be uncovered.

ACKNOWLEDGEMENT

The authors sincerely thank Greg Grason for the stimulating, in-depth discussion on the geometry of mesoatoms. KR and GD: This research was supported by NKFIH grants K149429 and EMMI FIKP grant VIZ. KR: This research has been supported by the program UNKP-24-3 funded by ITM and NKFI. The research was also supported by the Doctoral Excellence Fellowship Programme (DCEP) funded by ITM and NKFI and the Budapest University of Technology and Economics. The gift representing the Albrecht Science Fellowship is gratefully appreciated.

REFERENCES

- [1] G. Domokos, A. Goriely, Á. G. Horváth, and K. Regős. Soft cells and the geometry of seashells. *PNAS Nexus*, 3(9):pgae311, 2024.
- [2] Alan Schoen. Infinite periodic minimal surfaces without self-intersections. *Technical Note*, s2-43:NASA TN D-5541, 1970.
- [3] Gregory M. Grason and Edwin L. Thomas. How does your gyroid grow? a mesoatomic perspective on supramolecular, soft matter network crystals. *Physical Review Materials*, 7:045603, 2023.
- [4] H.A. Schwarz. *Gesammelte Mathematische Abhandlungen*. Berlin: Springer, 1933.

- [5] Lu Han and Shunai Che. An overview of materials with triply periodic minimal surfaces and related geometry: From biological structures to self-assembled systems. *Advanced Materials*, 30:1705708, 2018.
- [6] William Thomson. On the division of space with minimum partitional area. *The London, Edinburgh, and Dublin Philosophical Magazine and Journal of Science*, 24(151):503–514, 1887.
- [7] G.E. Budd. Morphospace. *Current Biology*, 31:R1141–R1224, Oct 2021.
- [8] M.I. Aroyo (ed). *International Tables for Crystallography, Volume A: Space-group symmetry*. International Union of Crystallography, 2016.
- [9] Alan L. Mackay. Periodic minimal surfaces. *Nature*, 314:604–606, 2015.
- [10] B. Riemann. über die fläche vom kleinsten inhalt bei gegebener begrenzung. *Abhandlungen der Königlischen Gesellschaft der Wissenschaften zu Göttingen*, 13:3–52, 1867.
- [11] P.J.F. Gandy and J. Klinowski. Exact computation of the triply periodic schwarz p minimal surface. *Chemical Physics Letters*, 322:579–586, 2000.
- [12] H.S.M. Coxeter. Regular skew polyhedra in three and four dimensions and their analogues. *Proceedings of the London Mathematical Society*, s2-43:33–62, 1936.
- [13] J.A.F. Plateau. *Statique Expérimentale et Théorique des Liquides soumis aux seules Forces Moléculaires*. Paris : Gauthier-Vilars, 1873.
- [14] D Weaire. Kelvin's foam structure: a commentary. *Phil. Mag. Letters*, 88(2):91–102, 2007.
- [15] R. Bitsche. Space-filling polyhedra as mechanical models for solidified dry foams. Master's thesis, Technical University of Vienna, 2005.
- [16] T. Daxner, R.D. Bitsche, and H.J. Böhm. Space-filling polyhedra as mechanical models for solidified dry foams. *Materials Transactions*, 47:2213–2218, 2006.
- [17] Ossian Bonnet. Deuxième note sur les surfaces a lignes de courbure sphériques. *C.R. Acad. Sci.Paris*, 36:389–391, 585–587, 1853.
- [18] H. Park, S. Jo, B. Kang, K. Hur, S.S. , Oh, D.Y. Ryu, and S. Lee. Block copolymer gyroids for nanophotonics: significance of lattice transformations. *Nanophotonics*, 11:2583–2615, 2022.
- [19] Wenpeng Shan and Edwin L. Thomas. Gradient transformation of the double gyroid to the double diamond in soft matter. *ACS Nano*, 18:9443–9450, 2024.
- [20] Á. G. Horváth. On the dirichlet—voronoi cell of unimodular lattices. *Geometriae Dedicata*, 63:183–191, 1996.
- [21] G.F. Voronoi. Nouvelles applications des paramètres continus à la théorie des formes quadratiques ii. *Geometriae Dedicata*, 136:67–181, 1909.

GÁBOR DOMOKOS, HUN-REN-BME MORPHODYNAMICS RESEARCH GROUP AND DEPT. OF MORPHOLOGY AND GEOMETRIC MODELING, BUDAPEST UNIVERSITY OF TECHNOLOGY, MŰEGYETEM RAKPART 1-3., BUDAPEST, HUNGARY, 1111

Email address: domokos@iit.bme.hu

ALAIN GORIELY, MATHEMATICAL INSTITUTE, UNIVERSITY OF OXFORD

Email address: goriely@maths.ox.ac.uk

ÁKOS G. HORVÁTH, HUN-REN-BME MORPHODYNAMICS RESEARCH GROUP AND DEPARTMENT OF ALGEBRA AND GEOMETRY, BUDAPEST UNIVERSITY OF TECHNOLOGY AND ECONOMICS, H-1111 BUDAPEST, MŰEGYETEM RKP 3.

Email address: ghorvath@math.bme.hu

KRISZTINA REGŐS, HUN-REN-BME MORPHODYNAMICS RESEARCH GROUP AND DEPT. OF MORPHOLOGY AND GEOMETRIC MODELING, BUDAPEST UNIVERSITY OF TECHNOLOGY, MŰEGYETEM RAKPART 1-3., BUDAPEST, HUNGARY, 1111

Email address: regoskriszti@gmail.com